Int. Journal of Refractory Metals and Hard Materials 42 (2014) 233–239

Contents lists available at ScienceDirect

Int. Journal of Refractory Metals and Hard Materials

journal homepage: www.elsevier.com/locate/IJRMHM

Fabrication of 93W–Ni–Fe alloy large-diameter rods by powder extrusion molding

Wensheng Liu, Qingshan Cai *, Yunzhu Ma, Qianfang Huang, Jiajia Zhang

State Key Laboratory of Powder Metallurgy, Central South University, Changsha 410083, PR China

ARTICLE INFO

Article history:
Received 21 July 2013
Accepted 14 September 2013

Keywords:
Powder extrusion molding
Tungsten heavy alloy
Binder
Solvent-thermal debinding
Extruded rod

ABSTRACT

A powder extrusion molding (PEM) process has been used for the manufacturing of tungsten heavy alloy rods with large length to diameter ratio. An improved wax-based multi-component binder was developed for PEM of 93W–Ni–Fe alloy. The miscibility of its components and the characteristics of the binder were evaluated and good thermal–physical properties were obtained. Also, the feedstock rheological properties, extrusion molding and debinding process were studied. The feedstock exhibited a pseudo-plastic flow behavior. The large length to diameter ratio rods, with diameters up to 36 mm were extruded at 65 °C by optimizing the extrusion process. A two-step debinding process was employed to remove the binder in the extruded rods. Solvent debinding was carried out in n-heptane at 45 °C to extract the soluble components. A process of repeated short time immersion and drying of the extruded rods (called short-period solvent debinding) was developed and using this novel technique the binder removed was raised from 45% to 60%. SEM analyses indicated that a large volume of pores was formed in debound rods, but had not created interpenetrating pore channels yet. The rest of the binder could be thermally extracted at a high heating rate without defects.

1. Introduction

Tungsten heavy alloys have excellent physical and mechanical properties. They are extensively used in the military field, e.g. kinetic energy penetrators. With the rapid development and innovation of tanks, armored vehicles and other defense equipments, higher demand for the strength and toughness and the length to diameter ratio of tungsten alloy materials for missiles (such as long rod penetrators) is required [1–3]. PEM is an advanced near net shape technology for powder metallurgy, which has been rapidly developed in recent years, and has now become one of the most effective ways to produce tube, rod, strip and other special shaped products of cemented carbide, high-density tungsten alloy, and other metals and their alloys [4–6].

The PEM process includes basically four steps: mixing, extrusion molding, debinding and sintering. Successful production of parts by PEM is closely related to the binder system utilized. However, little information has been reported concerning the PEM binder, especially for tungsten heavy alloys. In PEM, the binder should have low viscosity at the extrusion temperature, and good low-temperature fluidity during molding. During debinding, the binder should hold the shape and be totally removed with the least impact on the compact. To fulfill the above requirements a successful binder for the PEM process requires a multi-component mixture. Wax-based binders are often recommended because waxes have low-melting temperature, good wetting and low viscosity. Zhou et al. [4] have successfully manufactured hard-metal extruded rods with diameters up to 16 mm by using a novel wax-based binder system. Although wax-based binders are widely used, they suffer from long debinding time and a tendency to crack, slump or distort during debinding [7,8]. Thus, some of additives and modifiers are adopted to improve the comprehensive properties [9]. Moreover, debinding is the crucial step to limit the thickness and size of parts [10,11]. The current PEM or PIM (powder injection molding) technology can only fabricate parts with the thickness below 20 mm. If PEM binder can be designed comprehensively and the debinding cycles for PEM can be optimized, the PEM process can be suitable for fabricating larger-sized parts.

In this work, production of tungsten alloy rods via extrusion molding method with a developed wax-based binder was investigated. The rheology behavior of prepared feedstock was studied and extrusion molding was performed at low temperature. A combination of solvent debinding and thermal debinding was used for removing binder from specimens and defect free tungsten heavy alloy rods were manufactured after optimizing the process variables.

2. Experimental

2.1. Materials

The mixed 93W–4.9Ni–2.1Fe powder (Fig. 1) was used in the experiment. The characteristics of raw powders are listed in Table 1. The

* Corresponding author. Tel.: +86 0731 88877825.
E-mail address: cai2009pm@163.com (Q. Cai).

0263-4368/$ – see front matter © 2013 Elsevier Ltd. All rights reserved.
http://dx.doi.org/10.1016/j.ijrmhm.2013.09.011

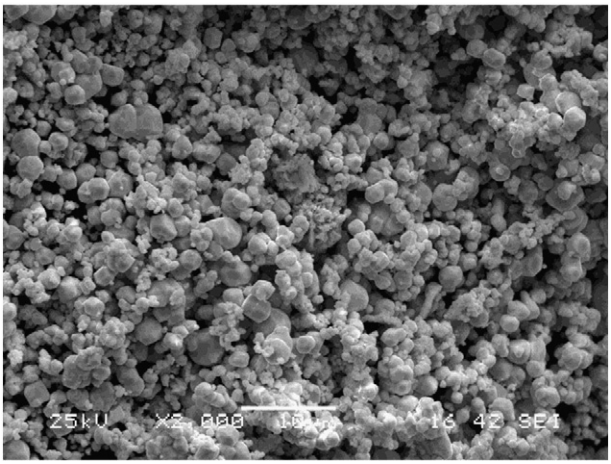

Fig. 1. SEM micrograph of 93W–4.9Ni–2.1Fe composite powder.

Fig. 2. A photograph showing the extrusion molding equipment.

binder used in this work was composed of paraffin wax (PW), liquid paraffin wax (LPW), high density polyethylene (HDPE), polyethylene vinyl acetates (EVA), carnauba wax (CW), stearic acid (SA) and a minor plasticizer (dioctyl phthalate, DOP) and modifier (polyethylene wax, PEW).

2.2. Process

The feedstock for extrusion was prepared by mixing a proper ratio of powder and binder. The proper ratio of the binder and tungsten heavy alloy powder was 50/50 by volume, respectively. Premixing was done with a dry-mixing apparatus (IJA, US) at room temperature (RT) and 30 r/min for 0.5 h. Fine mixing was done in a simple z-type stirring kneader (NH-20L, Jiangsu Province, China) at 160 °C and 41 r/min for 3 h. Green extruded rods were formed by extrusion molding the feedstock mixture in a Dorst vacuum worm type extrusion press using a water heating system (Fig. 2). The rods were cut into 80 mm sections to investigate the debinding character. Solvent debinding was carried out in n-heptane at different debinding temperatures (ranging from RT to 50 °C), in different periods (ranging from 2 to 16 h) and at fixed solvent feed ratio of 10/1 by volume. The rod samples (extrusion molded parts) were placed at the center of a 1500 ml self-designed device containing the solvent. The device was kept at a constant temperature by thermostatic water bath. The debound samples were air-dried to constant weight at RT.

The debinding ratio (W_d) was measured according to the following equation:

$$W_d = \frac{W_i - W}{W_i} \times 100 \quad (1)$$

where W_i is the initial weight of extruded body and W is the weight after solvent debinding. The binder removed weight fraction was calculated by dividing W_d by the total binder content (5 wt.%) in the feedstock.

After solvent debinding, the rods were thermally debound by using the designed heating curve, and then pre-sintered at 950 °C for 1 h in a vacuum debinding furnace. Sintering was performed under H_2 atmosphere in a molybdenum wire furnace.

Table 1
Typical characteristics of raw powder.

Powder	Powder shape	Particle size (μm)	Powder purity (%)
W	Irregular	2.0	99.9
Ni	Spherical	5–8	99.5
Fe	Irregular	5–8	99.5

2.3. Test methods

DSC and TGA analyses were used to study the thermal properties of the binder. The DSC and TGA experiments were performed on NETZSCH STA 449C under the following conditions: the heating rate was 10 °C/min, the atmosphere was pure nitrogen and the temperature was up to 600 °C. A capillary rheometer (Instron 3211) was used to measure the viscosity of the feedstock at 60–90 °C. A die with a diameter of 1.2 mm and a length of 51.0 mm was used. Photographs were taken for observation of the surface topography of the extrusion molding green rods. The surface morphology of the binder was observed with a polarizing microscope (OLYMPUS, PMG3). The sectional microstructures of the feedstock, green and debound rods were studied on a SEM device (JSM-5600LV, JEOL).

3. Results and discussion

3.1. Binder characterization

The thermal characteristics of the major binder components are summarized in Table 2. Various waxes and other adjuvants are added to the binder to lower down the viscosity and increase the miscibility, wettability and rheological property. To evaluate the performance of the binder, the extrusion property of the feedstock based on the binder was tested, and compared with a typical binder (see Section 3.2). The composition of the binders is listed in Table 3. The binder TB-1 is a typical wax-based binder for PIM tungsten heavy alloys [12,13] and an improved wax-based binder named NB-2 was developed for this work.

The prepared binder NB-2 was a light yellow hard solid at RT. After heating, an oil sticky and molten state substance was obtained. Fig. 3 shows the sectional SEM photographs of the prepared binder. This reveals that the binder has a uniform laminated structure. A typical polarizing microscope photograph is shown in Fig. 4. The white crystalline components (such as PW) are irregular lumps or fine particles, which has been dispersed uniformly in black amorphous components. The results show that the binder is simply a physical mixture of the components, suggesting partial miscibility, which is beneficial for each component to retain its specific feature.

Table 2
Thermal characteristics of binder components.

Binder component	Melting point (°C)	Weight loss start temperature (°C)	Rapid weight loss temperature (°C)	Weight loss end temperature (°C)
PW	58	160	230–350	510
LPW	–	70	180–270	450
HDPE	139	410	440–500	550
EVA	80	380	410–450	540
DOP	18	200	250–320	500

Table 3
Compositions of binder systems used in this study.

Binder ID	Component (wt.%)	Reference
TB-1	PW(74) + HDPE(5) + EVA(20) + SA(1)	[12,13]
NB-2	PW(55) + LPW(15) + CW(3) + HDPE(10) + EVA(10) + SA(1) + DOP(5) + PEW(1)	This work

DSC and TGA analyses were used to study the thermal characteristics of NB-2. It is found from Fig. 5 that there are two melting endothermic peaks at 58.7 °C and 117.0 °C, which are between the melting points of the binder components. DSC test demonstrates that good miscibility exists among the binder components. The TGA curve (Fig. 6) shows that the binder evaporates in two distinct temperature regions, which are in the temperature ranges from 200 to 385 °C and from 450 to 500 °C. This gradual and wide decomposition temperature range is beneficial for the debinding process.

3.2. Feedstock rheological properties and extrusion molding

The rheological properties of feedstock are crucial to evaluate the suitability for being extruded. The main problem in extruding large-diameter rods is the tendency to collapse. In this sense the rheological properties of the feedstock being extruded must be such that no deformation of the plastic green body can occur due to own weight or to the necessary handling [6]. To characterize the fluidity of the feedstock, its viscosity was measured at the extrusion temperature (60–90 °C) and shear rates in the range of 0–1500 s^{-1}. Fig. 7 gives the dependence of viscosity on shear rate for the prepared feedstocks based on the two binders. The feedstocks show pseudo-plastic behavior and the viscosity decreases with increasing shear rate. Also, as the temperature increases, there is a decrease in the feedstock viscosity. This behavior is the most adequate for the extrusion or injection process.

As it can be seen in Fig. 7, the flow behavior of the feedstock based on NB-2 is basically identical to the feedstock based on TB-1, but the values are reduced to some degree in all the shear rate range studied. This proves that the feedstock based on NB-2 has better rheological properties at low temperatures. The reason is that LPW and DOP added as modifier improve the rheology of the feedstock significantly [14]. From this point of view, the feedstock based on NB-2 was believed to be more suitable for extrusion molding step.

The feedstock present very good homogeneity as deduced from the microstructural analysis and from feedstock viscosity fluctuation with time. Fig. 8 shows a typical fracture surface of the feedstock (based on NB-2). It can be seen that the binder and powder are of good compatibility and the mixture is homogeneous. The SEM image shows a uniform distribution of the binder throughout the feedstock. A thin layer of the binder around almost all the particles can be seen, which is considered useful for facilitating the flow during the molding stage. Fig. 9 gives the viscosity variation with time at a constant shear rate of 1000 s^{-1}. Small variation of viscosity versus testing time indicates homogeneous feedstock [15].

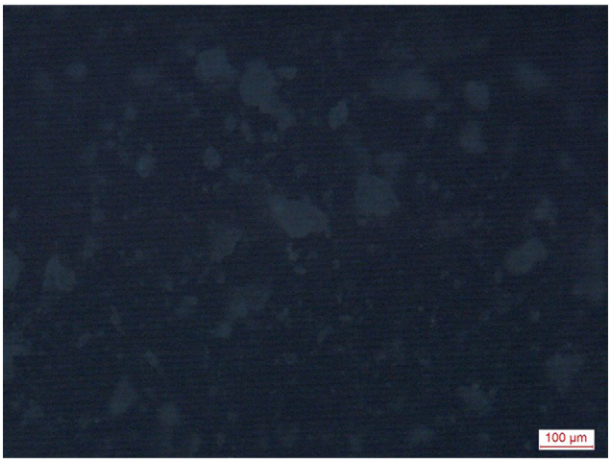

Fig. 4. Sectional polarizing microscope photograph of binder.

The molding properties of the prepared feedstocks were tested by the continuous extrusion experiment. The main factors that influence the quality of extruded rods include extrusion temperature and extrusion velocity. After repeated screening experiments, the optimal molding temperature for NB-2 based feedstock was determined to be 65 °C when the screw speed was 4.2 r/min, and the ratio between screw speed and feed speed was 2:1. The study showed that the high quality rods with good surface finish, and with diameters up to 24 mm and 36 mm were manufactured (Fig. 10). However, due to its high softening temperature, and its high viscosity and poor fluidity at low extrusion temperature, it is difficult for TB-1 based feedstock to form by this plastic extrusion process. That is, the traditional binder (TB-1) is only appropriate for PIM but not PEM.

3.3. Debinding process

Debinding is a critical and probably the most difficult step because it remains a challenge for thick samples to completely remove the binder without introducing defects such as cracking and blistering. A two-step debinding process, namely the solvent-thermal debinding method was used to extract the binders in the rods. The main advantage of this process is that the long debinding cycle in conventional thermal debinding

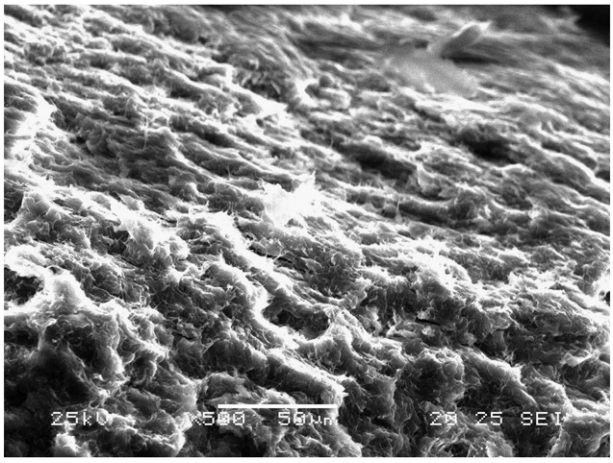

Fig. 3. Sectional SEM photograph of binder.

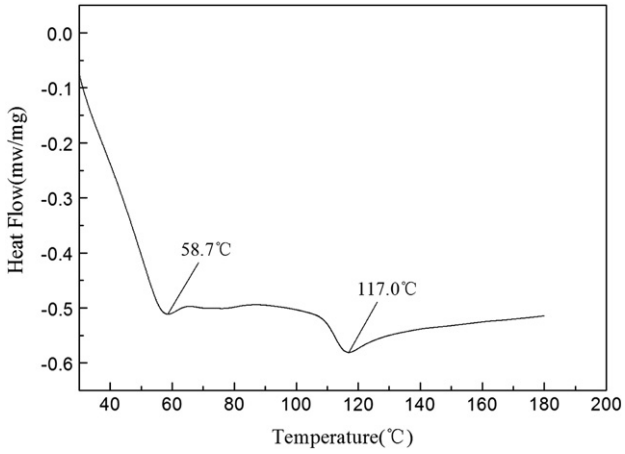

Fig. 5. DSC curve of binder.

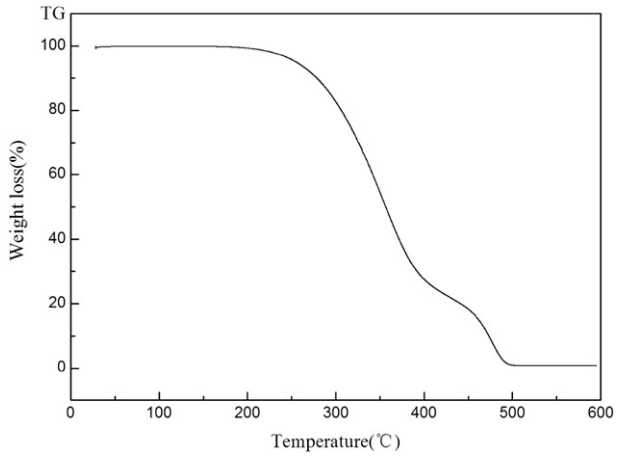

Fig. 6. TGA curve of the binder.

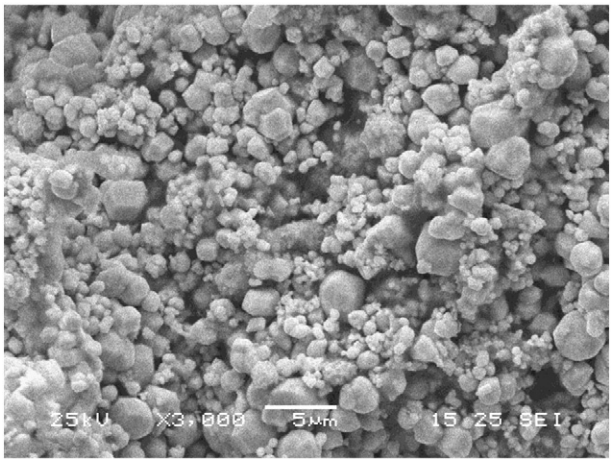

Fig. 8. SEM photograph of fracture of feedstock.

is now shortened significantly without causing cracking and distortion, which occur frequently in straight thermal debinding [16].

During the solvent debinding, the important parameters are debinding temperature and debinding time. Fig. 11 shows the temperature influence on the debinding process for Φ24 mm rods. The temperature promotes an improvement in debinding process efficiency for all specimen dimensions, due to an increase in solubility and diffusivity of soluble components (such as PW and LPW) in n-heptane as a function of temperature. A similar behavior has also been reported earlier in the literatures [11,17–19]. However, quite a number of the rods showed varying degrees of cracks or other defects within 12 h or shorter when the temperature rose to 50 °C. These defects are related to the swelling of the binder during solvent debinding, and the higher the temperature, the greater the possibility of the defects [20,21]. Fig. 12 shows the effect of debinding time on the binder removal at 45 °C for different sample thicknesses. After 16 h, the binder removed of Φ24 mm and Φ36 mm rods up to 55% and 45% were obtained, respectively. In general 79% of the soluble components (PW, LPW, CW, SA and DOP) could be extracted. But the debinding rods were suffering from cracking or slumping when the debinding time was over 18 h, which was also related to the binder swelling and softening. Therefore, the solvent debinding process for extruded rods, when not properly executed, may result in cracking, distortion, and slumping, which is attributed to binder swelling and binder softening, and the extent of swelling or softening increases with increasing temperature and debinding time. It can be seen from the above analysis that the most suitable solvent debinding condition is 45 °C for 16 h.

For safe and rapid binder removal with a minimum possibility of deformation and crack formation, the vacuum atmosphere was used in the subsequent thermal debinding process [8]. The rods that are solvent debound at 45 °C for 16 h have been thermally debound to remove the backbone components (HDPE, EVA and PEW) and the rest of the soluble components, which remain after solvent debinding. The thermal debinding cycles were performed based on the thermal decomposition of the binder components and the TGA curve of the binder (Fig. 13). After thermal debinding, defect-free Φ24 mm rods were gained, but serious crack and bubbling occurred in Φ36 mm rods (Fig. 14). That's due to the lower binder removed fraction of Φ36 mm rods during solvent

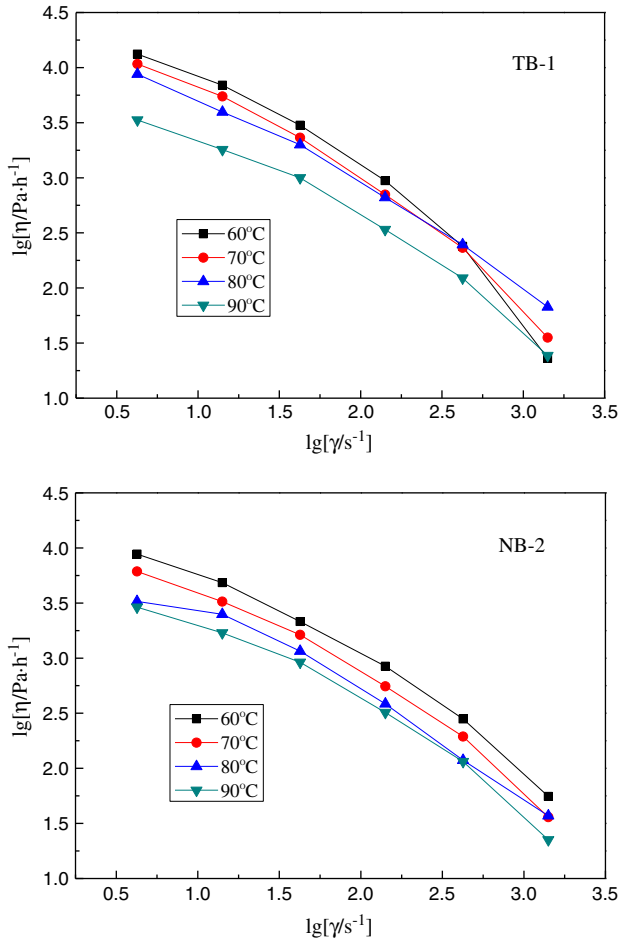

Fig. 7. Relationship between viscosity of feedstock and shear rate.

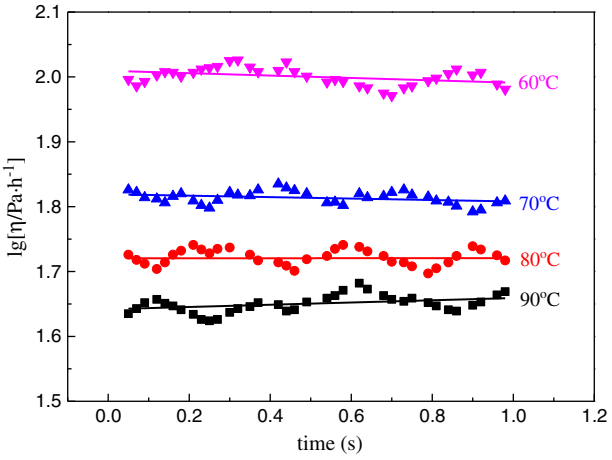

Fig. 9. Viscosity variation with time for feedstock at 1000 s^{-1}.

Fig. 10. Surface morphology of Φ24 mm and Φ36 mm green rods.

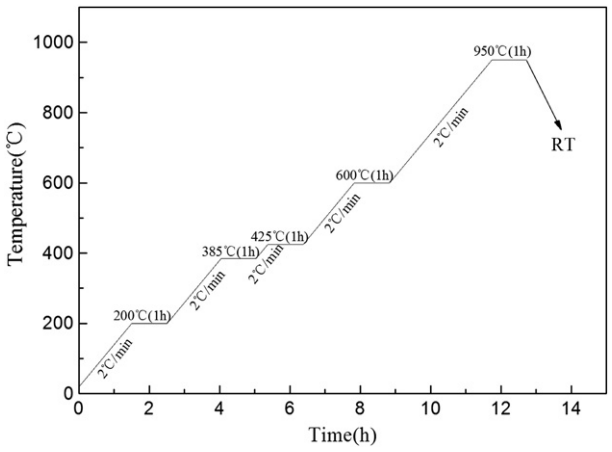

Fig. 13. Thermal debinding process.

debinding. Therefore, in order to avoid the defects that can be produced by inadequate binder removal, the binder removed fraction should be raised by optimizing the solvent debinding process.

Fig. 15 shows the sectional SEM photograph of the sample surface after solvent debinding, and it clearly displays the segregation phenomenon of some binder components. During the solvent debinding process, solvent molecules penetrate into the binder, producing swollen gels. Soluble binder components, such as PW, when dissolved in the solvent, would form liquid solutions, which have good fluidity [20]. So when taking samples out of the solvent debinding bath, and then air-drying them at RT, the liquid solutions would diffuse toward the surface due to the pressure and capillary force. A large quantity of liquid solutions was gathered together in the surface layers of rods, which would form an accumulation of binder as the solvent molecules began to evaporate. Since this

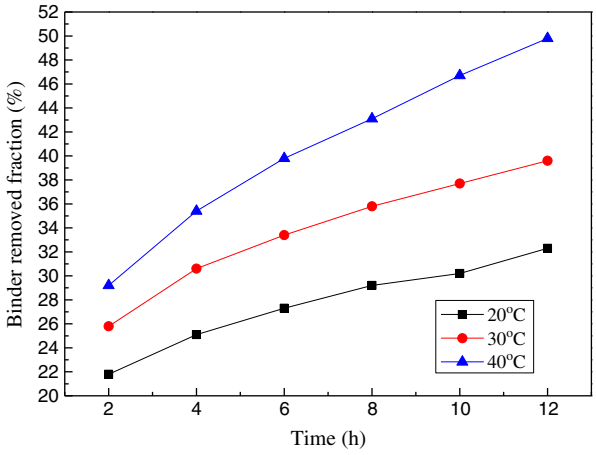

Fig. 11. Binder removed fraction at different debinding temperatures for Φ24 mm rods.

Fig. 14. Thermal debinding defects of Φ36 mm rod.

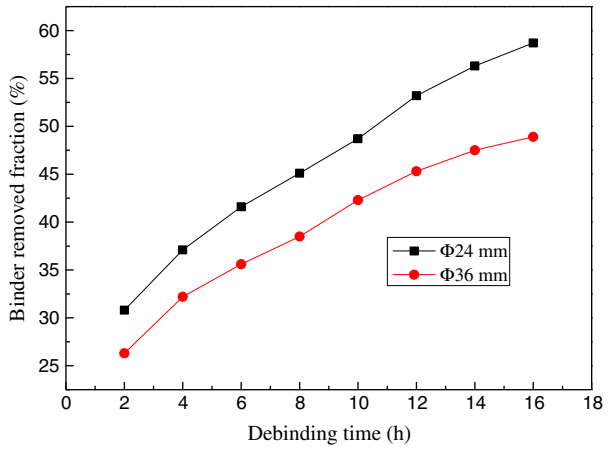

Fig. 12. Binder removed fraction at 45 °C for different sample thicknesses.

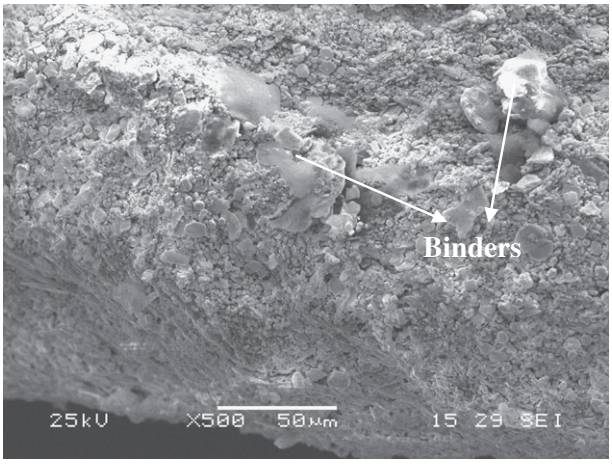

Fig. 15. SEM morphology of sample debound in axis direction.

part of residual binder could be removed quickly by immersing in the solvent again, a short-period immersing solvent method was designed as an optimized solvent debinding process for thick rods. The specific process was that first immersing in n-heptane at 45 °C for 12 h and drying at 40 °C for 1 h, then repeatedly re-immersing in n-heptane at 45 °C for 6 h and drying at 40 °C for 1 h. After immersing Φ36 mm rods in n-heptane for twice, around 60% of the soluble components have been removed. Therefore, during the optimized solvent debinding process, an intermediate stage was successfully introduced as an additional drying step to provide stress relaxation, and hence, no defects occurred. Furthermore, the rods had an adequate strength for handling even after solvent debinding.

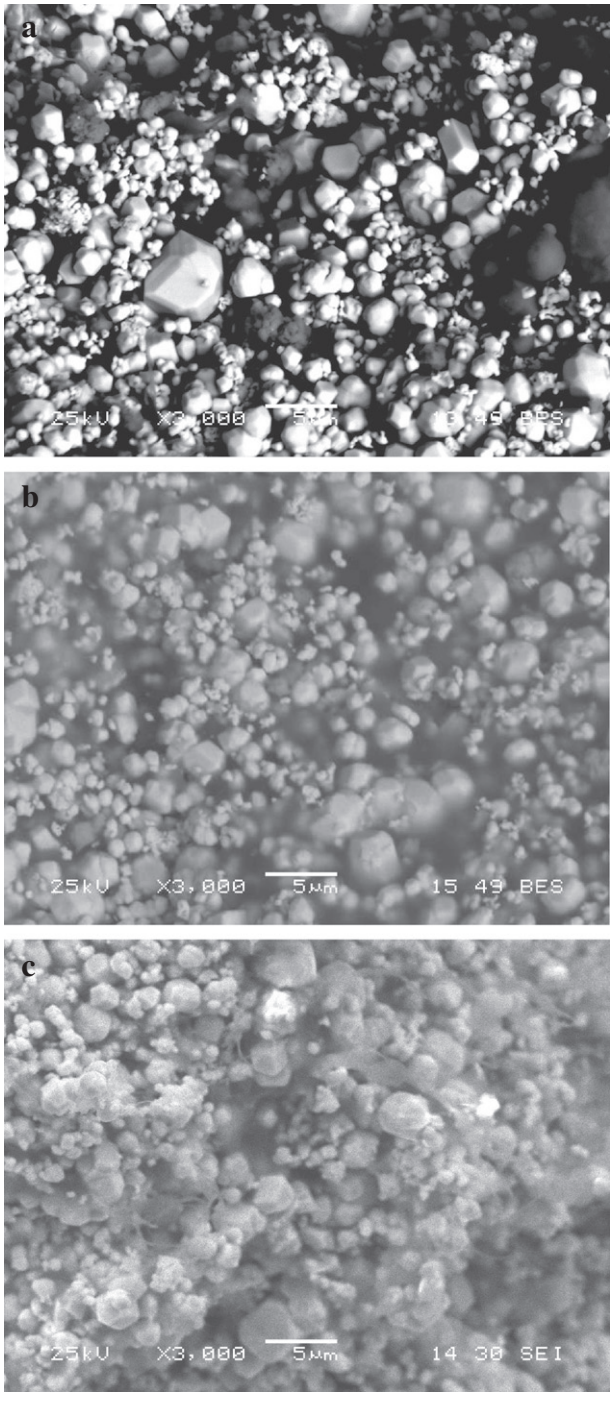

Fig. 16. SEM micrographs of solvent debound rod from surface (a) through (b) to center (c) of rod.

Fig. 16 shows the micrographs of Φ36 mm rod after immersion for twice. It reveals that the solvent debinding process is advancing from external to internal. There are a large amount of connected pores in the surface, and the morphologies of powder particles obtained became more distinct (Fig. 16a). With the formation of surface pores, the solvent gradually spread to the inside, the internal binder begins to dissolve, and forming a layer of medium similar to the "liquid film" which continuously distributed between the powder particles (Fig. 16b). However, there are still two-phase homogeneous mixtures of binder and powder in the center of debound rod (Fig. 16c). It can be seen that it is difficult for the thick samples to form interpenetrating pore channels from exterior to interior during solvent debinding. However, Since nearly 60% of binder was removed by optimizing solvent debinding process in the present study, there is a large volume of capillary porosity inside of rod which makes leaving of gaseous products in subsequent thermal debinding easy in short time. After thermal debinding, the rest of the binder (nearly 40%) was removed. The total weight loss percent of these rods was close to 5%, indicative of a successful debinding process. After sintering at 1550 °C for 180 min in reductive H_2 atmosphere, rods free of defect were obtained. Fig. 17 shows a photograph of the sintered rods after the surface machining process.

4. Conclusions

A wax-based multi-component binder for extrusion molding of tungsten heavy alloy has been developed and tested. The polarizing microscope, SEM and DSC analyses showed that this binder system has good miscibility and thermal properties which are beneficial for the debinding process. The rheological characteristic of feedstock allowed to perform the extrusion molding at relatively low temperatures, as well as a pseudo-plastic behavior favoring the molding process. The defect-free 93W–Ni–Fe green rods were obtained at an extrusion temperature of 65 °C. A short-period solvent debinding method was successfully introduced as an optimization solvent debinding process for thick rods to raise the binder removed fraction and to avoid the debinding defects. By optimizing the solvent-thermal debinding process conditions, tungsten heavy alloy extruded rods with diameters of up to 36 mm, with no defects, were manufactured successfully.

Acknowledgments

The author thanks the National Natural Science Foundation of China (No. 50774098) and the Creative Research Group of National Natural Science Foundation of China (Grant No. 50721003) for financial support.

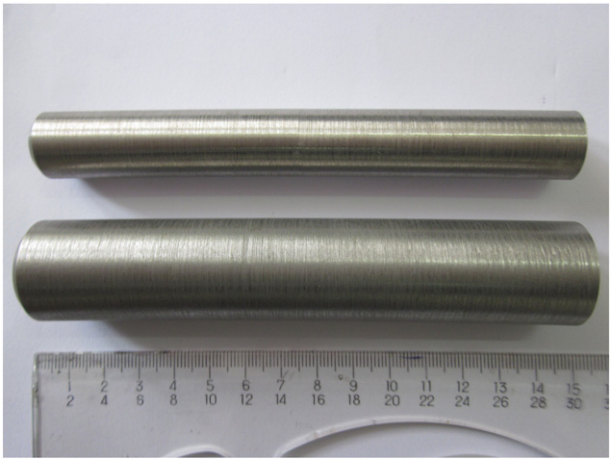

Fig. 17. Photograph of Φ24 mm and Φ36 mm sintered rods.

References

[1] Li JR, Yu JL, Wei ZG. Influence of specimen geometry on adiabatic shear instability of tungsten heavy alloys. Int J Impact Eng 2003;28(3):303–14.
[2] Pedersen B, Bless S. Behind-armor debris from the impact of hypervelocity tungsten penetrators. Int J Impact Eng 2006;33(1–12):605–14.
[3] Liden E, Andersson O, Lundberg B. Deformation and fracture of a long-rod projectile induced by an oblique moving plate: experimental tests. Int J Impact Eng 2011;38(12):989–1000.
[4] Zhou JC, Huang BY, Wu EX. Extrusion moulding of hard-metal powder using a novel binder system. J Mater Process Technol 2003;137(1):21–3.
[5] Sotomayor ME, Levenfeld B, Varez A. Powder extrusion moulding of 430L stainless steel thin tubes for porous metal supported SOFCs. Powder Metall 2011;54(2):103–7.
[6] Jardiel T, Levenfeld B, Jimenez R, Varez A. Fabrication of 8-YSZ thin-wall tubes by powder extrusion moulding for SOFC electrolytes. Ceram Int 2009;35(6):2329–35.
[7] Tseng WJ, Hsu CK. Cracking defect and porosity evolution during thermal debinding in ceramic injection moldings. Ceram Int 1999;25(5):461–6.
[8] Liu XQ, Li YM, Yue JL, Luo FH. Deformation behavior and strength evolution of MIM compacts during thermal debinding. Trans Nonferrous Met Soc China 2008;18(12):278–84.
[9] German RM, Bose A. Injection molding of metals and ceramics. Princeton, NJ: Metal Powder Industries Federation; 1997.
[10] Li YM, Jiang F, Zhao LG, Huang BY. Critical thickness in binder removal process for injection molded compacts. Mater Sci Eng A 2003;362(1–2):292–9.
[11] Zaky MT, Soliman FS, Farag AS. Influence of paraffin wax characteristics on the formulation of wax-based binders and their debinding from green molded parts using two comparative techniques. J Mater Process Technol 2009;209(18–19):5981–9.
[12] Fan JL, Huang BY, Qu XH. MIM of mechanically alloyed nanoscale W–Ni–Fe powder. Int J Powder Metall 2002;38(6):56–61.
[13] Ye HZ, Liu XY, Hong HP. Fabrication of metal matrix composites by metal injection molding—a review. J Mater Process Technol 2008;200(1–3):12–24.
[14] Zhu BJ, Qu XH, Tao Y. Powder injection molding of WC-8%Co tungsten cemented carbide. Int J Refract Met Hard Mater 2002;20(5–6):389–94.
[15] Aggarwal G, Park S, Smid I. Development of niobium powder injection molding: part I. Feedstock and injection molding. Int J Refract Met Hard Mater 2006;24(3):253–62.
[16] Hwang KS, Hsieh YM. Comparative study of pore structure evolution during solvent and thermal debinding of powder injection molded parts. Metall Mater Trans A 1996;27(2):245–53.
[17] Oliveira RVB, Soldi V, Fredel MC, Pires ATN. Ceramic injection moulding: influence of specimen dimensions and temperature on solvent debinding kinetics. J Mater Process Technol 2005;160(2):213–20.
[18] Zaky MT. Effect of solvent debinding variables on the shape maintenance of green molded bodies. J Mater Sci 2004;39(10):3397–402.
[19] Onbattuvelli VP, Enneti RK, Park SJ, Atre SV. The effects of nanoparticle addition on binder removal from injection molded aluminum nitride. Int J Refract Met Hard Mater 2013;36:77–84.
[20] Thomas Vielma P, Cervera A, Levenfeld B, Varez A. Production of alumina parts by powder injection molding with a binder system based on high density polyethylene. J Eur Ceram Soc 2008;28(4):763–71.
[21] Lin HK, Hwang KS. In situ dimensional changes of powder injection-molded compacts during solvent debinding. Acta Mater 1998;46(12):4303–9.